Available online at www.sciencedirect.com
ScienceDirect
Nuclear Physics B (Proc. Suppl.) 212–213 (2011) 59–67
NUCLEAR PHYSICS B PROCEEDINGS SUPPLEMENTS
www.elsevier.com/locate/npbps

The ARGO-YBJ contribution to the cosmic ray physics

Michele Iacovacci[a], on behalf of the ARGO-YBJ Collaboration

[a]INFN and University of Napoli, Complesso Universitario MSA, Via Cintia, 80126 Napoli, Italy

The ARGO-YBJ experiment is in stable data taking since November 2007 at the YangBaJing Cosmic Ray Laboratory (Tibet, P.R.China, 4300 m a.s.l.). It exploits a full coverage and high altitude approach to the small air showers detection. The detector is made of a single layer of RPCs operated in streamer mode, fully instrumenting a central carpet of about 5700 m^2, then a guard ring extends the partially instrumented area to about 11,000 m^2. The large field of view (~ 2 sr) and the high duty cycle ($\geq 85\%$) allow a continuous monitoring of the sky in the declination band from -10° to 70°; the detector operates with an energy threshold of a few hundred GeV. Recent achieved results will be reported.

1. Introduction

The ARGO-YBJ experiment is currently the only air shower array exploiting the full coverage approach at high altitude, with the aim of studying the cosmic radiation at an energy threshold of a few hundred GeV. With its high duty cycle and wide field of view, the apparatus can cope with both transient phenomena and long term monitoring of astrophysical object. The high altitude and the detector features make ARGO-YBJ capable of investigating a wide range of fundamental issues in Astroparticle Physics, namely:
- very high energy gamma-ray astronomy, with an energy threshold of a few hundreds GeV;
- search for gamma ray bursts in the full GeV-TeV energy range;
- study of cosmic rays (spectrum, composition, $\bar{p}$/ratio ratio measurement, anisotropy) starting at TeV energies;
- Sun and heliosphere physics above GeV energies.

In the following sections, after a brief description of the experiment, recent results achieved on the above mentioned items will be presented and discussed.

2. The ARGO-YBJ experiment

The detector is composed of a central carpet large $\sim 74 \times 78$ m^2, made of a single layer of Resistive Plate Chambers (RPCs) with ∼93% of active area, enclosed by a guard ring partially (∼20%) instrumented up to $\sim 100 \times 110$ m^2. The apparatus has modular structure, the basic data acquisition element being a cluster (5.7×7.6 m^2), made of 12 RPCs (2.8×1.25 m^2 each). Each chamber is read by 80 external strips of 6.75×61.8 cm^2 (the spatial pixels), logically organized in 10 independent pads of 55.6×61.8 cm^2 which represent the time pixels of the detector. In order to extend the dynamic range up to PeV energies, a charge read-out has been implemented by instrumenting each RPC with two large size pads (BigPad), of dimensions 139×123 cm^2, acting as pick up electrodes. The RPCs are operated in streamer mode by using a gas mixture (Ar 15%, Isobutane 10%, TetraFluoroEthane 75%) for high altitude operation. The high voltage set at 7.2 kV ensures an overall efficiency of about 96% [6]. The central carpet contains 130 clusters while the guard ring, made of 23 clusters, enlarges the instrumented area so allowing a better shower reconstruction. A manifold coincidence ($\geq N_{trig}$) of fired pads of the central carpet (N_{pad}), in a time window of 420 ns, implements the inclusive trigger that starts the event data acquisition. At $N_{pad} \geq N_{trig} = 20$ the rate of random coincidences is still the negligible and data are almost free from spurious hits. The apparatus, in its full configuration of 153 clusters, is in smooth and stable data taking since November 2007 with the trigger threshold $N_{trig} = 20$; the trigger rate is $\sim$ 3.6 kHz with a dead time of 4%.

0920-5632/$ – see front matter
doi:10.1016/j.nuclphysbps.2011.03.008

3. Long-term monitoring of Mrk421

The Mrk421 high variability makes the long term multiwavelength observation very important to constrain the emission mechanisms models. Thanks to its high duty cycle and wide field of view, ARGO-YBJ has monitored Mrk421 for more than 2 years, studying the correlation of the TeV flux with X-ray emission. In Fig.1 the

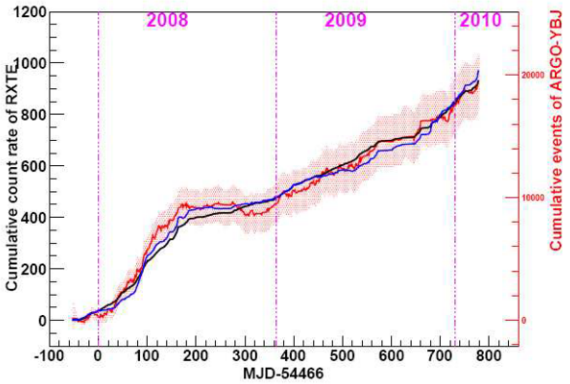

Figure 1. Mrk421 cumulative light curve. Red line: rate of TeV gamma rays measured by ARGO-YBJ. The red band indicates the statistical error of one standard deviation. Black line: soft X-rays by RXTE/ASM. Blue line: hard X-rays by Swift/BAT.

ARGO-YBJ observation of Mrk421 from November 2007 to February 2010, in correlation with the X-ray data of RXTE/ASM (2-12 keV) and Swift/BAT (15-50 keV) is shown. The integrated flux of ARGO-YBJ refers to showers with $N_{pad} > 60$ on the central carpet and zenith angle less than 45°, that means photons with a median energy of 1.1 TeV if a power law spectrum with index -2.4 is assumed. A cumulative signal of 11 standard deviations has been observed by ARGO-YBJ in 676 days; the data set used to correlate TeV gamma ray and X-ray emissions consists in 566 days of simultaneous observations. A clear correlation between cumulative counts of X-ray and ARGO-YBJ integrated flux is visible in Fig.1. In order to quantify the degree of correlation and to show a possible time lag between gamma and X-ray emissions, the discrete correlation function (DCF)[27] has been used. It comes out the maximum correlation to be well consistent with no time lag. In order to perform a differential analysis, the data have been divided in 4 groups, according to the X-ray rate measured by RXTE/ASM; we found that the correlation between gamma ray and X-ray fluxes is more consistent with a quadratic relation rather than linear (see Fig.2). Studying the average energy spectra of each group, both for ARGO-YBJ and RXTE/ASM, the data show an evident positive correlation between the flux and the spectrum hardness. In particular the index of the ARGO-YBJ spectrum increases from -2.48±0.22 to -1.87±0.21 when the flux (E > 1 TeV) increases from 0.9 to 7 Crab units, in agreement with a previous measurement of the Whipple experiment [20], suggesting that this is a long term property of the source.

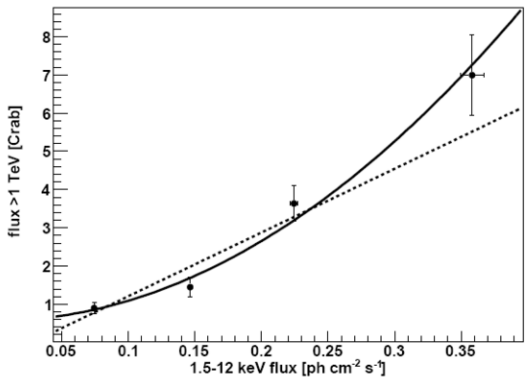

Figure 2. Mrk421 gamma ray flux (E > 1 TeV) vs. X-ray flux (E=1.5-12 keV). The dashed and solid lines are the linear and quadratic fit of the data points, respectively.

4. MGRO J1908+06

At the ARGO-YBJ site, MGRO J1908+06 culminates at the relatively low zenith angle of 24° and is visible for 5.4 hours per day with a zenith angle less than 45°. The data-set used to this analysis [4] contains all showers with zenith angle less than 45° and $N_{pad} > 40$ recorded in the period from November 2007 to March 2010, for a total of 730.5 days. The analysis method is the standard search for point gamma ray sources [2] with an optimization of the observational windows radius due to the extension of the source. To evaluate the extension, for simplicity, we assumed a source shape described by a symmetrical 2-dimensional Gauss function with r.s.m $= \sigma_{ext}$, independent of the gamma ray energy. Fitting the event distribution as a function of the distance from the center (set to the Fermi pulsar position [12]) and taking into account the detector PSF, we found $\sigma_{ext} = 0.48^{+26}_{-28}$, a value larger but consistent with the HESS measurement [7]. Using the measured extension, we calculated by simulation the optimal window size in order to get the best signal to noise ratio. The significance map in Fig.3 shows an area of excesses, with statistical significance greater than 4 s.d., near the location of the Fermi pulsar, in particular closer to the positions reported by MILAGRO and HESS. The maximum significance in the region is 4.7 s.d.. For the spectrum determination we assumed a simple power law dependence: $dN/dE = KE^{-\gamma}$, without cutoff. To study the spectral behavior we defined 4 N_{pad} intervals: 40-99, 100-299, 300-999 and > 1000. Then we compared the rate observed in each interval with the rate given by a simulation assuming a set of test spectra. The best fit power law spectrum is: $dN/dE = 3.6^{+0.7}_{-0.8} \times 10^{-13}(E/6TeV)^{-2.2^{+0.34}_{-0.29}}$ photons $cm^{-2}s^{-1}TeV^{-1}$ (the errors on the parameters are purely statistical). The systematic errors are mainly related to the background evaluation and to the uncertainty in the absolute energy scale. According to our estimate, they globally affect the quoted flux by less than 30%. To check the existence of a cutoff, we fit the data with a power law spectrum multiplied by the exponential factor $\exp(E/E_{cut})$, varying E_{cut} 1 to 50 TeV.

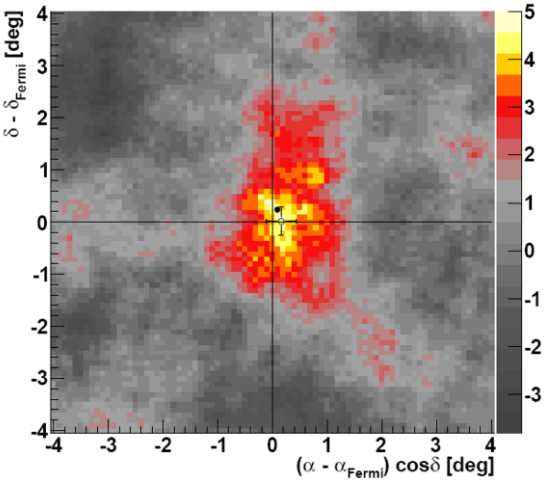

Figure 3. Significance map of the region around MGROJ1908+06 obtained by ARGO-YBJ, for events with $N_{pad} > 100$. The center of the map represents the position of the Fermi pulsar 0FGL J1907.5+0602. The open and solid circle show the positions measured respectively by MILAGRO and HESS.

Decreasing the value of E_{cut}, the best fit gives a spectrum with an increasingly flatter slope; however the value of the χ^2 remains minimum for a spectrum with no cutoff. The found spectrum is shown in Fig.4, together with the spectra by MILAGRO and HESS. The Crab Nebula spectrum [2] is reported for comparison. Given its slope, the MGROJ1908+06 flux becomes larger than the Crab Nebula one just above a few TeV . A significant disagreement appears between the ARGO-YBJ and HESS spectra. Concerning ARGO-YBJ and MILAGRO, considering the large errors in the flux measurements (the error on the MILAGRO flux is about 30% at 10 TeV and larger at lower energy), the apparent disagreement could be likely due to statistical fluctuations. In conclusion, in the limit of the statistical accuracy of this result, our data supports the MILAGRO measurement of a flux significantly larger than the one measured by HESS.

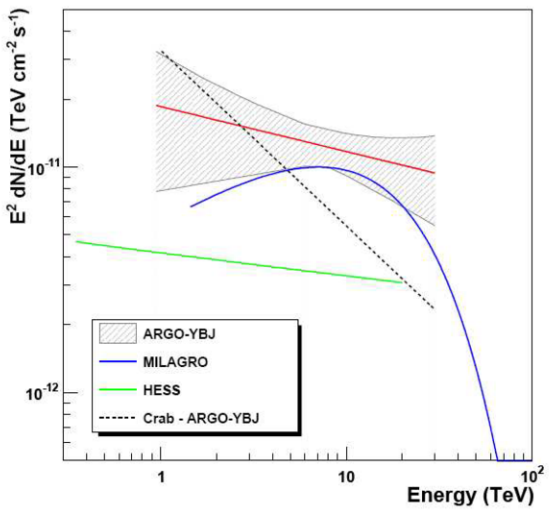

Figure 4. Gamma ray flux from MGRO J1908+06 measured by ARGO-YBJ (red line) multiplied by E2. The shaded band represents 1 standard deviation error. The blue and green lines show the flux measured by MILAGRO and HESS, respectively. The black dashed line represents the Crab Nebula flux.

5. Interplanetary magnetic field measurement by Sun shadow

Cosmic rays arrive mostly isotropically at the Earth and can be recorded by detectors on ground. Those coming from the Sun direction are absorbed and form a clear deficit, or a shadow, in a uniform sky map. The Interplanetary Magnetic Field (IMF) deflects the cosmic rays along their path to the earth and shifts the Sun shadow from its true position.

Its y-component, B_y, defined as lying in the ecliptic plane and perpendicular to the line of sight Sun-Earth, moves the Sun shadow in the north-south direction. At the YBJ site, the geomagnetic field has a declination angle which is less than 0.5°, therefore it does not contribute to the north-south shift of the Sun shadow. Using this effect, ARGO-YBJ has measured B_y in the period July 2006 to October 2009, when the solar activity stayed at its minimum for an unexpectedly long time. This a particularly good time window and fits the stability requirement of B_y, in fact the IMF is better studied in a quiet phase of the Sun as it is strongly modulated by the solar activity. Using this data set,namely 903 exposure days in total, the map of the sun shadow has a maximum significance of 45 s.d. located at $(0.17\pm0.02)^\circ$ toward north and $(0.26\pm0.02)^\circ$ toward west. By fitting the measured Sun displacement as a function of the solar longitude, one can estimate B_y,with a minimal assumption on its model [28,21]. For cosmic rays composition, which has to be considered in simulating the Sun shadow displacement, it has been taken into account that measured in balloon experiments [1]. Data have been grouped in two sub-sample, namely G1 (January 2008 to April 2009) and G2, where G1 contains data with the IMF showing a bisector structure, while G2 all the others. This classification has been done according to the Sun shadow behavior as measured in our data, but we could check that our classification was confirmed by satellite-borne detectors [18]. Then, the Sun shadow displacement has been plotted versus the solar longitude, or the Carrington period (27.3 days) which is the time we need to observe one complete Sun rotation, and finally the B_y value extracted according to the simple model in [28,21]. The results are shown in Fig.5: the solid curves, with uncertainty represented by the shaded area, are the results of the ARGO-YBJ experiment while the solid dots represent the measurements by the orbiting detectors [18]. The two measurements are of the same order in the amplitude of (2.0 ± 0.2) nT and are consistent in the alternating periodical pattern, even though the two profiles are shifted with each other by about 2 days due to the different speed of the solar wind (400 km/s), which transports the field, and of the TeV particles ($\sim c$) we measure. Therefore, even more importantly, this measurement could foresee fluctuations of IMF which will sweep the earth about 2 days later, demonstrating a potential forecasting capability for magnetic storms due to solar events.

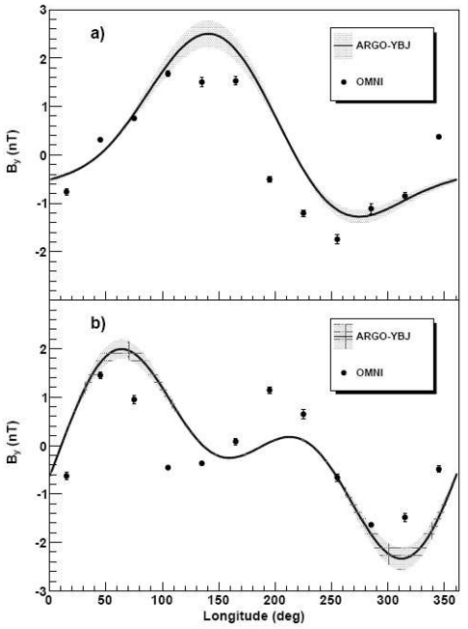

Figure 5. The solid curve represents the B_y component of IMF field as measured by the ARGO-YBJ near the earth; the shaded area corresponds to an uncertainty of one standard deviation. In the upper panel a), corresponding to period G1 (see text), a clear bisector pattern is observed. The solid dots represent the measurements using the OMNI observational data downloaded from [18]. In the lower panel b), the results with the 4-sector structure in period G2 are displayed.

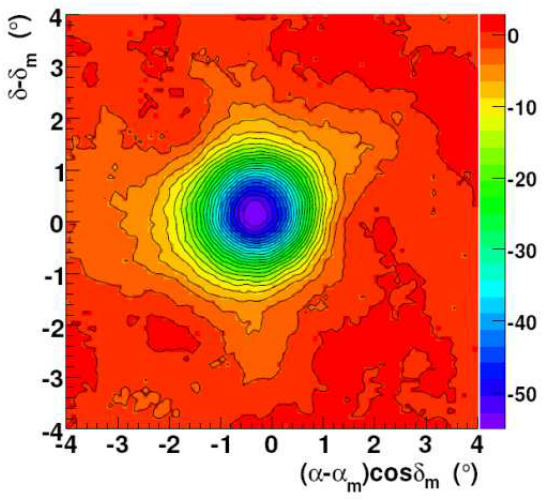

Figure 6. Moon shadow significance map for events with $N_{pad} \geq 100$ fired pads. The color corresponds to the statistical significance according to the color scale on the right, where the correspondence is with the number of s.d..

6. $\bar{p}/p$ ratio measurement by Moon shadow

As for the Sun, a similar deficit of the cosmic ray flux is observed in the Moon direction. Fig.6 shows the statistical significance map of the Moon region. With all data from July 2006 to December 2009 (about 3200 hours on-source in total) we observed the cosmic ray Moon shadowing effect with a significance of about 55 s.d.. Two ranges of pad multiplicity have been chosen to the antiproton abundance measurement, namely $40 \leq N_{pad} < 100$ and $N_{pad} \geq 100$. In the former bin the statistical significance of the Moon shadow deficit is 34 s.d., the measured angular resolution is about 1°, the proton median energy is 1.4 TeV and the number of missing events about 183000. In the latter multiplicity bin the significance is 55 s.d., the measured angular resolution about 0.6°, the proton median energy is 5 TeV and the number of missing events about 46500. The accuracy of the energy scale determination is estimated to be less than 18% in the energy range $1-30$ TeV/Z . Using all data collected until November 2009, we set two upper limits on the $\bar{p}/p$ flux ratio [3]: 5% at an energy of 1.4 TeV and 6% at 5 TeV with a 90% confidence level. In the few-TeV range the ARGO-YBJ results are the lowest available, useful to constrain models for antiproton production.

7. Anisotropy

Observation of the sidereal cosmic ray anisotropy at energies of 1 - 100 TeV is a useful tool in probing the magnetic field structure in our

interstellar neighborhood as well as the distribution of sources. Cosmic-rays at these energies are almost entirely of Galactic origin and are expected to be nearly isotropic due to interactions with the Galactic magnetic field [26].

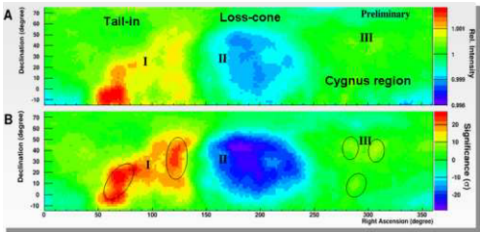

Figure 7. Large scale cosmic-ray anisotropy observed by ARGO-YBJ at energies of $\sim$ 2 TeV . In the upper plot the color scale gives the relative cosmic-ray intensity, in the lower plot the statistical significance in standard deviations.

ARGO has measured a large scale anisotropy [11] as shown in Fig.7 where three distinct regions, respectively labeled as I, II and III , are reported. The region I is the spread excess area called "Tail-in", which is composed of two small discrete regions with peak significance of about 20. s.d. and a relative intensity the order of 0.1%. Region II is a large deficit area, identified as "Loss-cone"; last, the excess in Region III, which is close to the Cygnus region.

To quantify the scale of anisotropy the 1-dimensional R.A. projections of the 2-dimensional maps have been fitted with the first two harmonics at three different energies. The preliminary results on amplitude (A_1) and phase ϕ_1 of the first harmonic, shown in Tab.1, are in good agreement with other experiments [14]. The heliosphere is suggested to be responsible for the "Tail-in" excess and the local interstellar MF for the "Loss-cone" deficit [23]. However, it is argued that the observation of Multi-TeV anisotropy does not favour this interpretation, as the heliosphere cannot influence cosmic-rays with energy larger than 10 TeV [15,22]. The discrete distribution of cosmic-ray sources is another possible cause.

E (TeV)	A_1	ϕ_1 (°)
0.7	$(3.6 \pm 0.1) \cdot 10^{-4}$	(63.4 ± 0.9)
1.5	$(6.8 \pm 0.1) \cdot 10^{-4}$	(41.0 ± 0.7)
3.9	$(9.0 \pm 0.1) \cdot 10^{-4}$	(35.3 ± 0.6)

Table 1
Values of amplitude and phase of the first harmonic from the fit of the 1-dimensional R.A. projection.

As to the intermediate scale, the two anisotropy hot spots in Region I reported by Milagro at 10 TeV [13], have been observed, at 2 TeV, also by the ARGO-YBJ detector [8]. The two excesses (Fig.8) have significance greater than 10 s.d. and correspond to a flux increase of about 0.1%. The origin of these regions is not understood yet, although they have been identified as local excesses of cosmic rays. Besides conventional explanations related to the Galactic or local magnetic field, further possibilities have been suggested, like the Geminga pulsar acting as a local cosmic-ray source or magnetic mirror effect produced by a local cosmic-ray source.

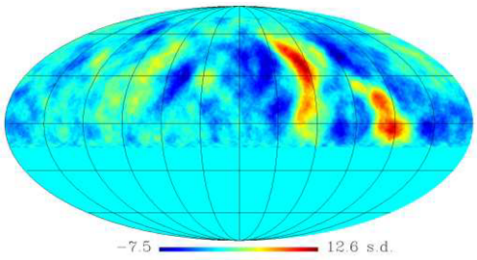

Figure 8. Medium scale anisotropy of cosmic-rays at energies $\sim$ 2 TeV. The colour scale gives the statistical significance in standard deviations.

8. Measurement of the light component of cosmic rays in the 5–250 TeV region

By using a Bayesian approach, a measurement of the light-component spectrum of the primary cosmic rays, in the energy region (5–250) TeV, has been performed. Data belong to the period January - May 2008.

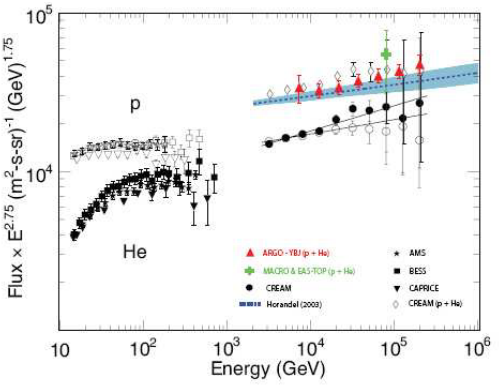

Figure 9. The differential energy spectrum of the light-component (proton and helium) measured by ARGO-YBJ (filled triangles) compared to the proton spectrum (open circles) and helium spectrum (filled circles) measured by the CREAM experiment [1].

The energy spectrum was obtained through the Bayesian unfolding procedure [24] applied to our data. A full detector simulation was performed in order to evaluate the relevant quantities needed by the unfolding procedure. The results are shown in Fig.9. The measured spectrum refers to the energy region 5–250 TeV. The results are affected by a statistical error the order of 1%. Sources of systematic errors taken into account in the analysis where: a) the selection cuts on the measured quantities; b) the uncertainties of the detector response; c) effects related to the ratio of helium component used to evaluate the Bayesian probabilities. We estimated the result to be affected by a total uncertainty the order of 10% The contributions of elements heavier than helium nuclei to the energy spectrum have been estimated to be negligible. The results have been compared both to the recent results of the CREAM experiment and to the best fit provided by Horandel for the proton and helium experimental fluxes [19]. The point at 80 TeV represents the "p + He" intensity measured by the EAS-TOP and MACRO experiments [17], at the Gran Sasso Laboratory, by combining the quantities simultaneously measured by different detectors, namely the electromagnetic component of the shower , the Cerenkov light and the high energy muons. We concluded the light component spectrum to be flatter than in the lower energy region, so adding evidence to the hardening observed in cosmic-ray elemental spectra by CREAM.

9. Approaching higher energies with the analog readout

The RPC charge readout [10], which is in operation on the entire central carpet since December 2009, extends the energy range of measurement, allowing the study of cosmic radiation up to PeV energies. Fig.10 shows two showers as seen by the analog readout system. In the vertical scale is the ADC count of each BigPad (see text) which is about 1.7 m^2; as the system can be operated at different density scales, two cases are reported, namely: upper panel a), the ADC full scale corresponds to about 6500 particles/m^2; lower panel b), the ADC full scale corresponds to about 1300 particles/m^2. According to simulations, the two showers would roughly correspond to a primary proton of about 1 PeV in a) and to a primary proton of 200 -300 TeV in b). It is quite impressive the regularity of the density profile. We stress that no experiment has ever measured very close to the shower core with such a detail. The centrality-dependent dijet asymmetry measured at LHC in Pb-Pb collisions at $\sqrt{s_{NN}} = 2.76$ with the ATLAS detector ([5] and references therein), makes the core region even more interesting. Owing to the analog readout the the proton-air cross section and the inferred p-p cross section, already measured in the 1 - 200 TeV energy region [9], will

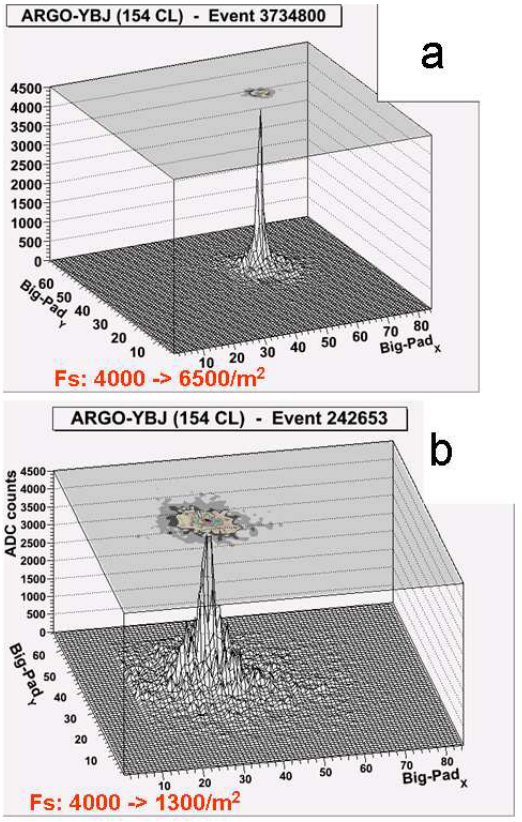

Figure 10. Showers as recorded by ARGO-YBJ through the Analog Readout system. The reference energies are respectively, about 1 PeV in a) and 200 - 300 TeV in b) (see text).

be extended to the PeV energies, as well as the composition measurements.

10. Conclusions

Recent achievements of ARGO-YBJ on gamma ray astronomy have been reported. The long term monitoring on Mrk421 around TeV energies is quite a unique result. The IMF measurement has been performed with a very high precision so demonstrating the forecast capability of this measurement. The ARGO-YBJ results on $\bar{p}$ content of cosmic rays are already able to constrain models for antiproton production. The already measured anisotropy of cosmic rays and the detector features, namely lower energy threshold, good angular resolution and high duty cycle, make us confident about the possibility of further digging in this intriguing subject, looking for discovery of finer details . The measured composition of the light component confirms the hardening of the spectrum and outline a more detailed picture the cosmic rays. All together, these and the already published results, especially on Gamma Ray Burst and p-p cross section, establish ARGO-YBJ as a quite successful multipurpose experiment.

REFERENCES

1. Ahn, H.S., et al., 2010, ApJ , 714, L89.
2. Aielli, G., et al., 2010, ApJ, 714, L208.
3. Di Sciascio,G. and Iuppa, R., theese proceedings.
4. Vernetto, S., et al., 2010, Proc. 22nd ECRS, Turku, Finland.
5. Aad, G., et al., 2010, arXiv:1011.6182v2
6. Aielli, G., et al., 2009, NIM A, 608, 246.
7. Aharonian, F., et al. 2009, Astron. Astrophys, 499, 723.
8. Vernetto, S., et al. 2009, Proc. 31.th ICRC, Lodz, Poland.
9. G.Aielli et al., 2000, Phys. Rev. D, 80, 092004.
10. Iacovacci, M., et al., 2009, Proc. 31.th ICRC, Lodz, Poland.
11. Zhang, J.L., et al., 2009, Proc. 31.th ICRC, Lodz, Poland.
12. Abdo, A.A., et al., 2009, ApJL, 700, L27.
13. Abdo, A.A., et al., 2008, Physical Review Letters, 101, 221101.
14. Guillian, G., et al., 2007, Phys. Rev. D, 75, 062003.
15. Amenomori, M., et al., 2006, Science, 314, 439.
16. Amenomori, M., et al., 2005, ApJ, 633, 1005.
17. Aglietta, M., et al., 2004, Astropart. Phys., 21, 223.
18. King, J.H. and Papitashvili, N. E., 2004, J. Geophys. Res., 110, A02209, 10.1029/2004JA 010804; corresponding data are available at http://omniweb.gsfc.nasa.gov/

19. Horandel, J.R., 2003, Astropart. Phys., 19 193.
20. Krennrich, F., et al.(2002), ApJ, 575, L9.
21. Amenomori, M., et al., 2000, ApJ, 541, 1051.
22. Hall, D.L., et al., 1999, JGR 104, 6737.
23. Nagashima, K., et al., 1998, Journal of Geophysical Res.,103,17429.
24. D'Agostini, G., 1995, Nucl. Instrum. Meth. A, 362, 487.
25. Alexandreas, D.E., et al., 1993, NIM A, 328, 570.
26. Berezinskii, V. S., Bulanov, S. V., Dogiel, V. A., and Ptuskin, V. S. 1990, Astrophysics of Cosmic Rays (Amsterdam: North-Holland).
27. Edelson, R.R., Krolik, H.J., 1988, ApJ, 333, 646.
28. Parker, E. N., 1963, Interplanetary Dynamical Process, VIII, InterScience, New York